University of Szeged
Faculty of Science and Informatics
Department of Physical Geography and Geoinformatics

Dr. Boudewijn van Leeuwen
Assistant professor

Continuous monitoring of inland excess water using medium resolution active and passive satellite data

Habilitation thesis

Szeged
2020

1. Introduction

Temporary inundations of large parts of the flat areas on the Carpathian Basin cause serious financial, environmental and social problems. On the contrary to riverine and coastal floods, these floods occur when – due to limited runoff, infiltration and evaporation – the superfluous water remains on the surface, or at places where groundwater – flowing towards lower areas – appears on the surface by leakage through porous soil. In literature, these inundations are often identified as inland excess water (IEW)[1], surface ponding, areal flood, or surface water flood (Rakonczai et al. 2011, Szatmári & Van Leeuwen 2013). In Hungary, more than 24% of the arable land is in areas moderately or highly endangered by inland excess water. The temporal distribution of IEW in Hungary is erratic and difficult to predict (Figure 1.)
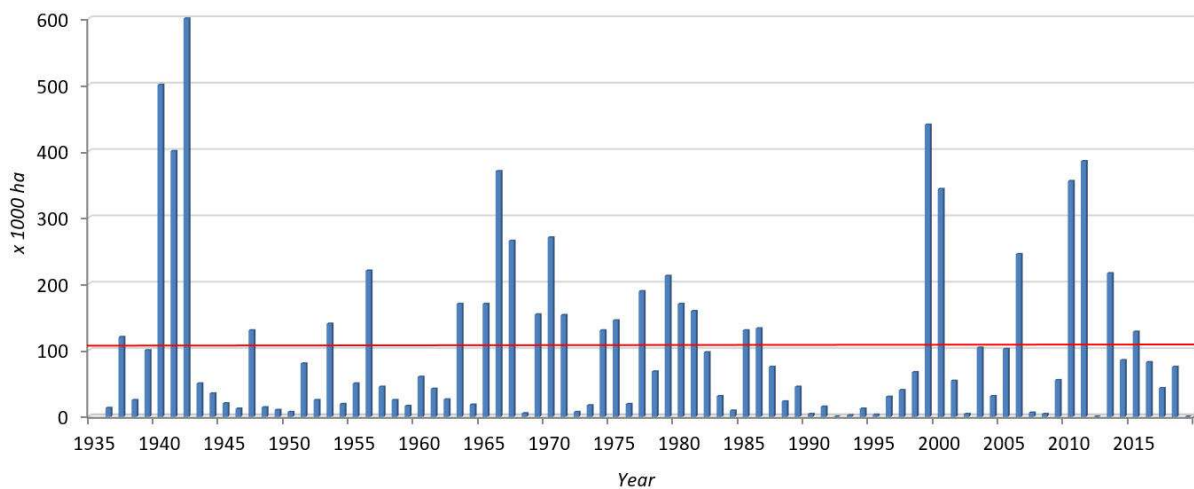

Figure 1. Maximum (blue bars) and average (red line) area covered by inland excess water in Hungary between 1935 and 2019. Except for the year 1940-1944, the inundations from before 1950 are estimates (Sources: Pálfai 2000, Official IEW report on vizugy.hu).

The IEW problem is not new; already in the 19th century, it was mentioned as a natural hazard (Pálfai 2001). Many engineers and scientists have worked to find solutions to reduce the damage due to the extreme amount of water. Before it is possible to take action against the problem, it is necessary to understand the phenomenon and identify the factors and processes that cause the formation of inland excess water. Also, it is important to determine the location and size of the inundations to be able to take operative measures to mitigate and prevent further damage. When it is precisely known where and when IEW occurs, it may be possible to forecast the location, size and duration of future floods and to develop preventive policies. One of the potential solutions to the inland excess water problem is to store the surplus water in reservoirs or natural wetlands for later periods of drought (Kozák 2006). Many climate change models predict higher variability of precipitation and that extremely intensive precipitation will occur more often in the Carpathian Basin, especially in Spring and early Summer, while drought may develop during different periods in the same year (Mezosi et al. 2013). For such complex water management, it is important to understand where and why IEW develops.

---

[1] The floods are called *Belvíz* in Hungarian, but there is no formally accepted definition (Pálfai 2001) nor translation to English for the concept. In literature, both *excess water* and *inland water* can be found, but are not used here since *inland water* may cover any type of water that is not sea or ocean, while *excess water* may also describe inundations due to flooding rivers (Van Leeuwen 2012). *Standing water* or *sitting water* are terms that are usually used for smaller areas, up to about 100 m^2 that are temporarily covered by water. In this habilitation thesis, *inland excess water* will be used since it attributes to the surplus nature and the geographical location of the floods.

Four major approaches to map and monitor IEW can be identified (Van Leeuwen et al. 2017). The oldest approach is the *visual observation* of inland excess water patches. The first in-situ inland excess water maps in Hungary date from during the Second World War. Since then, observations have been carried out during every rainy period in areas affected by IEW. This approach is labor intensive and can easily result in errors due to misinterpretation and differences in observation methodology (Van Leeuwen et al. 2013). Aggregating the in-situ maps over time can be useful to create maps showing the vulnerability to inland excess water floods at an approximate scale of 1:100 000. Monitoring is not possible using the field observations, since normally only the maximum observed inundation during an IEW period is drawn on the map.

Pálfai was one of the first to perform *hazard mapping* based on factors causing inland excess water resulting in the national inland excess water index map (Pálfai 2003). Since then, many national, regional and local versions of this approach have been published (e.g. Bozán et al. 2005, Bozán et al. 2009, Pásztor et al. 2015, Bozán et al. 2017, Bozán et al. 2018, Nađ et al. 2018). The maps provide information on the vulnerability of an area to IEW, but do not give information about actual occurrences, nor about the development of the phenomenon.

Modelling of inland excess water has been proposed using *hydrological modelling* software as well (Van Leeuwen et al. 2016, Kozma 2019). Van Leeuwen et al. 2016 shows that this approach can result in detailed models of the inundations, but requires large amounts of accurate input data, which is often only available for very small areas.

The fourth approach to *map and monitor IEW is based on remote sensing data and algorithms*. Data collected from small (drones), medium (aerial photographs) and large (satellite imagery) areas have been used to detect inland excess water (Van Leeuwen et al. 2020a). The fields of remote sensing and image processing provide a large set of well understood methods that can be applied in a standardized method allowing to create uniform IEW maps of large areas with good spatial resolution. Data from different passive sensors have been extensively used for this purpose, for example Licskó et al. 1987, Csornai et al. 2000, Rakonczai et al. 2001, Mucsi & Henits 2010, Van Leeuwen et al. 2012, Van Leeuwen et al. 2013, Csendes & Mucsi 2016, Balázs et al. 2018, Szatmári et al. 2020, Van Leeuwen et al. 2020b). The disadvantage of passive remote sensing data is its limited usability during bad weather conditions which are often present during IEW periods. Therefore, approaches using active satellite data to detect IEW or other shallow temporal water bodies have been published as well (Csornai et al. 2000, Baghdadi et al. 2001, Csekő 2003, Manjusree et al. 2012, Gálya et al. 2016, Liu 2016, Van Leeuwen et al. 2017, Gulácsi et al. 2019). In general, radar data has been used for water, and especially flood identification in many studies. For example, Bolano et al. (Bolanos et al. 2016) developed a method to detect open water bodies using a dual threshold method with high resolution Radarsat 2 data. Also, approaches of combined monitoring of surface water with optical and radar data have appeared (Hong et al. 2015, Binh Pham-Duc et al. 2017).

With the development of ESA's Copernicus program, a large fleet of satellites has been launched that provide data for a large range of applications. The Sentinel-1 satellites have been among the first platforms in the program and provide data using an active remote sensing instrument. The data set is an improvement over earlier radar data sets like ERS and Radarsat, because it provides continues, near global data with a high temporal interval (Malenovský et al. 2012). The Sentinel-2 satellites in the constellation provide medium resolution multispectral data with a high temporal interval as well. The combined use of Sentinel-1 and Sentinel-2 data has been studied for different applications, like land use / land cover classification (Clerici et al. 2017, Steinhausen et al. 2018, Tavares et al. 2019) and wetlands mapping (Chatziantoniou et al. 2017). Although flood detection based on Sentinel-2 has been studied before (Goffi et al. 2020, Slagter et al. 2020), a fully automated approach based on the combination of Sentinel-1 and -2 data to determine the extent of non-permanent shallow water bodies has not yet been published.

This habilitation thesis summarizes my inland excess water related research since my PhD work. It is the result of my continuous study to improve IEW mapping using satellite imagery. The thesis presents a complex algorithm based on freely available Sentinel-1A and Sentinel-1B radar data, and Sentinel-2A and Sentinel-2B multispectral data that can be used to derived accurate weekly inland excess water maps at regional or national scale.

2. Study area and data

2.1. Study area

The weekly IEW monitoring algorithm can be applied to any area but here the results for a 5913 km^2 large area in the southeast of the Great Hungary Plain, enclosed by the Tisza, Körös and Maros rivers and the Hungarian-Romanian border is shown (Figure 2).
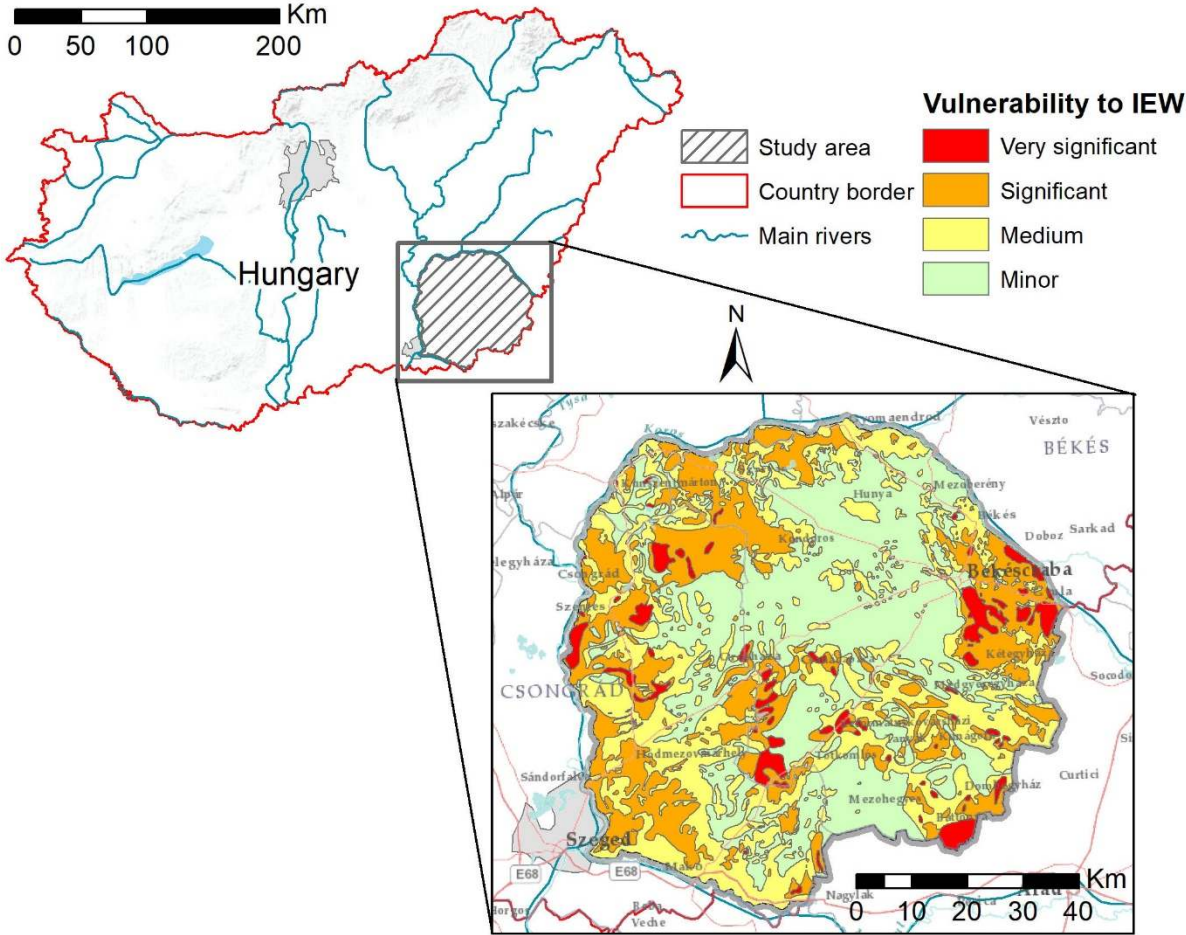

Figure 2. Study area of inland excess water mapping and its vulnerability (according Pálfai 2003).

This region has similar characteristics as the study areas that were used in my earlier research (Van Leeuwen et al. 2013, Tobak et al. 2014a, Tobak et al. 2014b, Van Leeuwen & Tobak 2014, Van Leeuwen et al. 2016, Van Leeuwen et al. 2017, Ladányi et al. 2019, Tobak et al. 2019, Van Leeuwen et al. 2020a). The elevation is between 77 and 107 meter (above Baltic mean sea level). The areas that are most vulnerable are south of the city of Orosháza, the low-lying plains in the west, the valley of the lower Tisza and the areas close to the Körös river. There is a close relation between these areas and the

regularly flooded regions prior to the 19th century river regulations (Bozán et al. 2018). Due to the geomorphological characteristics of the Maros alluvial fan, also on the higher areas inland excess water can develop, which can cause significant damage at the border of the alluvial fan (Rakonczai 2011). The development of inland excess water in this area is favored because 84% of the soils are clayey and 50% of them have poor water absorption and unfavorable water management characteristics, and their upper, middle, and lower layers are easily saturated. Eighty-eight percent of the agricultural land is arable land, which is because more than 75% of the soils are fertile chernozem. Five percent of the land cover in the study area is urban.

The development of IEW is closely, but not exclusively, related to the period with high precipitation in January - March, therefore the research period is focused on resp. March 2016 and March 2018. In 2016, during the period between January and March the precipitation was continuously above the 1971-2000 long term average for that period, while in February, it was even twice as high as normally. After the high precipitation period in the second half of February, between March 14-20, just before and during the satellite data acquisition, also quite some rain fell. The temperature of 5-10° C was several degrees above the normal temperature in February and March, causing increased evaporation (Van Leeuwen et al. 2020a).

In February 2016, everywhere on the Great Hungarian Plain inland excess water developed. In March, IEW in Hungary peaked at a maximum 82 427 ha (Integrált vízháztartási tájékoztató Aprilis 2016). The year 2016 can be considered a moderate year in terms of total area in Hungary covered by IEW (Van Leeuwen et al. 2020a)

In February, as well as in March 2018, the precipitation was twice as high as the national long-term average between 1971–2000 for those months. In fact, in the south part of the study area, the precipitation was already above the seasonal average in January. At the end of February, a cold period with precipitation started, which resulted in a considerable layer of snow. The warmer period in the middle of March caused the snow to melt and the soil to get saturated by melting water. Also, substantial rainfall fell during March, especially on the 18th (Van Leeuwen et al. 2020a). Satellite imagery from March 28, 29, 30 and 31 used in the study shows the development of IEW at the end of March. The total area covered by IEW in Hungary was with 73 184 ha (Integrált vízháztartási tájékoztató Aprilis 2018) slightly less than in 2016. This year should also be considered a moderate IEW year.

2.2. Data

The inland excess water mapping workflow integrates different remote sensing datasets with auxiliary vector and raster data. The satellite images were obtained from the scientific data hub of the Copernicus Earth observation program of ESA (ESA Sentinel Scientific Data Hub. 2020).

2.2.1. Sentinel satellite data

Sentinel-1 satellite constellation offers C-band radar data, day and night, and under all weather conditions. At the study area, the two satellites provide images about every third day in 3 descending and 2 ascending paths (Figure 3). The applied Interferometric Wide (IW) swath mode covers a 250 km width area and has 5 x 20 meter spatial resolution. In total 9, Level 1 Ground Range Detected (GRD) products, containing both Vertical – Vertical (VV) and Vertical – Horizontal (VH) polarizations were automatically downloaded for the study period in 2016. Twenty-one images were downloaded for the study period in 2018 (Table 1).

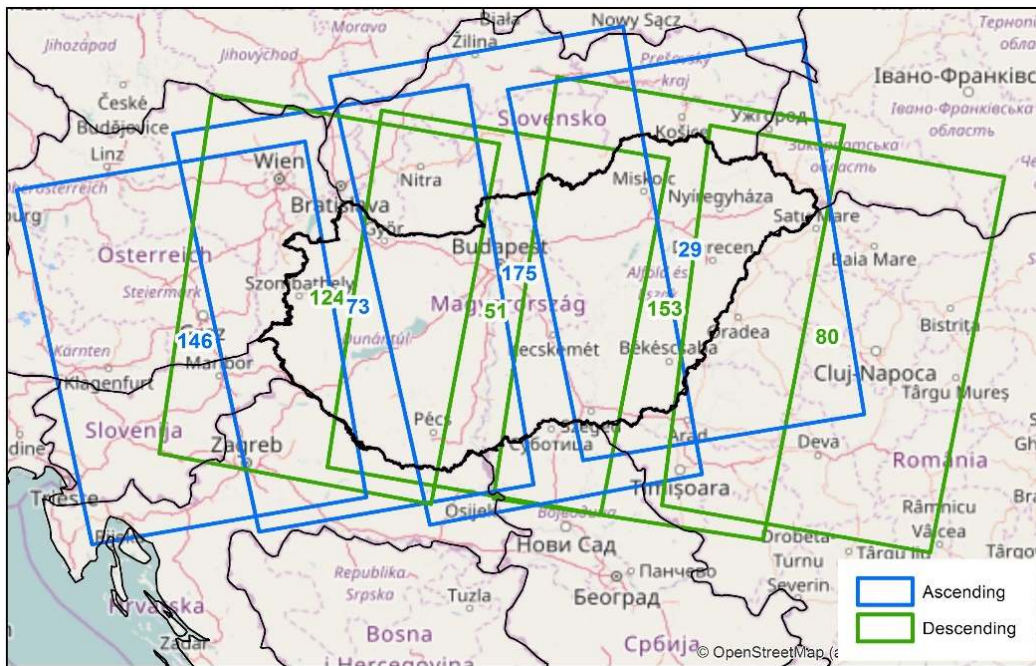| Satellite / Sensor	Date	Polarization	Spatial resolution / coverage
Sentinel-1A / 1B	16 March 2016		
	20 March 2016		5 x 20 m (resampled to 10 x 10 m)
		C-band (5,405 GHz)	
	28 March 2018	VV / VH	250 km width
	29 March 2018		
	30 March 2018		
	31 March 2018		

Table 1. Sentinel-1 input data.

Figure 3. Sentinel-1 data available for Hungary (Van Leeuwen et al. 2017).

Sentinel-2 multispectral satellites provide optical data with a 5-day revisiting period. From the available 13 spectral bands, covering the spectra from the visible part through near infrared to short-wave infrared, only 10 bands with 10 and 20 meter spatial resolution were used in the analysis (Table 2). For the first study period in 2016, only the Sentinel-2A satellite was in orbit and just the Level 1C (L1C, Top-of-Atmosphere) data product was available for download. In 2018, also data from Sentinel-2B, at Level 2A (L2A, Bottom-of-Atmosphere (BoA) reflectance values) was accessible. In the Sentinel-2 granule system, the study area is fully covered by four 100 x 100 km tiles: 34TDT, 34TDS, 34TET, 34TES (Figure 2). Altogether, 30 tiles of the optical images from six different dates were processed.

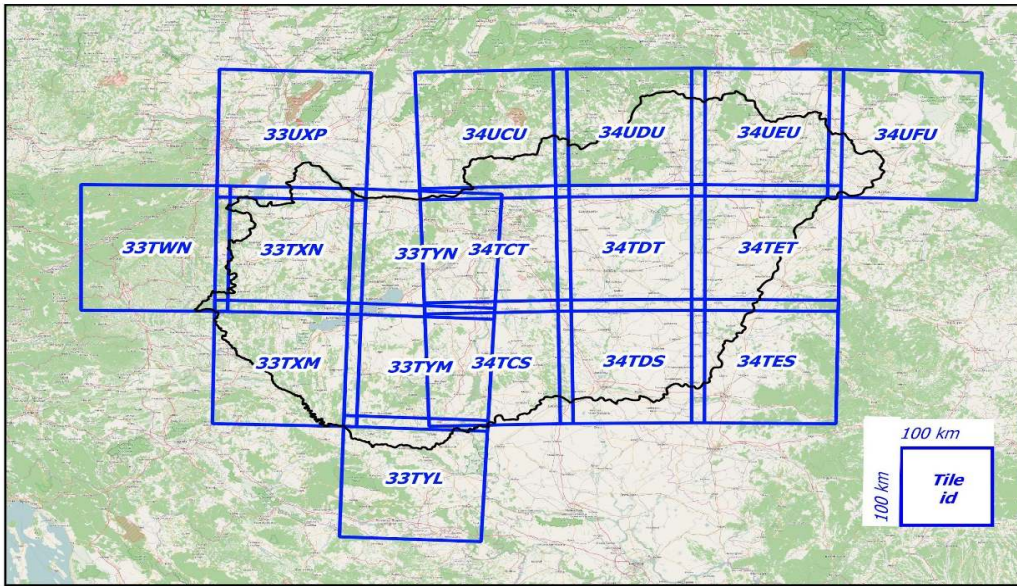| Satellite / Sensor	Date	Spectral bands	Spatial resolution / coverage
Sentinel-2A / 2B	16 March 2016		
	20 March 2016	B2: 492.4 / 492.1 nm	10 m (B2, B3, B4, B8)
		B3: 559.8 / 559.0 nm	
	28 March 2018	B4: 664.6 / 664.9 nm	20 m (B5, B6, B7, B8A, B11, B12)
	29 March 2018	B5: 704.1 / 703.8 nm	
	30 March 2018	B6: 740.5 / 739.1 nm	
	31 March 2018		

Table 2. Sentinel-2 input data.

Figure 4. Sentinel-2 data available for Hungary in the 100x100 km granule system (Van Leeuwen et al. 2017).

2.2.2. Validation data

In the validation process, independent remote sensing data, acquired with satellite and aerial sensors, were used (Table 3). In 2016, reference data of IEW patches were generated from a SPOT-7 high-resolution image. In 2018, an orthophoto was used to create the reference data set. The spatial resolution of the orthorectified SPOT-7 image is 1.5 m due to pan sharpening of the original 6 meter multispectral bands. The image covers an area of 400 km^2 on the NW part of the study area (Figure 5). Aerial photographs were taken with a 60 MP RGB camera deployed on a Cessna 172 airplane. The generated orthophoto mosaic covers an area of approximately 20 km^2 in the NW of the study area.

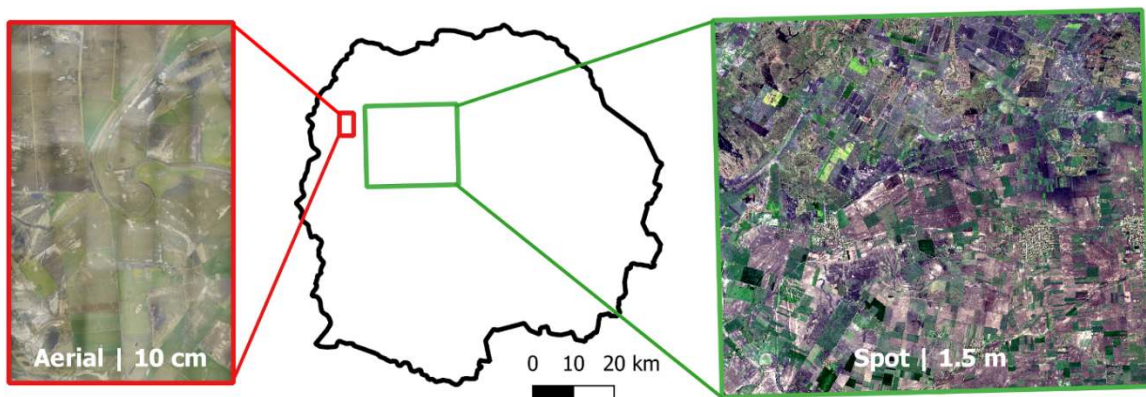| Satellite / Sensor	Date	Spectral bands	Spatial resolution / coverage
SPOT 7	14 March 2016	Blue: 450 / 520 nm Green: 530 / 590 nm Red: 625 / 695 nm Near Infrared: 760 / 890 nm	1.5 m 400 km^2
PhaseOne P65+	28 March 2018	RGB	10 cm 20 km^2

Table 3 Validation data sets

Figure 5. Validation sites on the study area.

2.2.3. Auxiliary data

The satellite data-based algorithm requires two mask files to identify and evaluate inland excess water inundations. The first mask was initially derived from vector maps stored in the hydro-geographic database of the General Directorate of Water Management and stores permanent water bodies, like lakes and rivers that were used as reference areas to detect water using the three algorithms of the workflow to identify pixels with water. Manually update using very high-resolution satellite images stored in Google Earth was required to improve the accuracy of the mask. In total, 1400 ha of reference pixels was extracted evenly spread over the study area. A second mask was created to limit the area where the algorithm can detect IEW. This mask is based on the National High Resolution Layer (nHRL) and the hydro-geographic database. It is used to exclude permanent water bodies, built up areas, anthropogenic land cover like large roads, railroads and large buildings. In this way, 12% of the study area is excluded for evaluation as possible IEW.

3. Methodology

The aim of the methodology was to create inland excess water maps for very large (regional, national) areas. My earlier research showed that data often was missing or that the accuracy of the results was very low if the extent of IEW was determined based only on one image (Van Leeuwen et al. 2017). Therefore, the algorithm was designed to collect and evaluate all optical and radar images for the area within a seven-day period. To create the resulting weekly inland excess water map, a large number of images is required, and multiple parallel workflows had to be developed. The final algorithm was based on the integration of the results of three workflows (Figure 6).
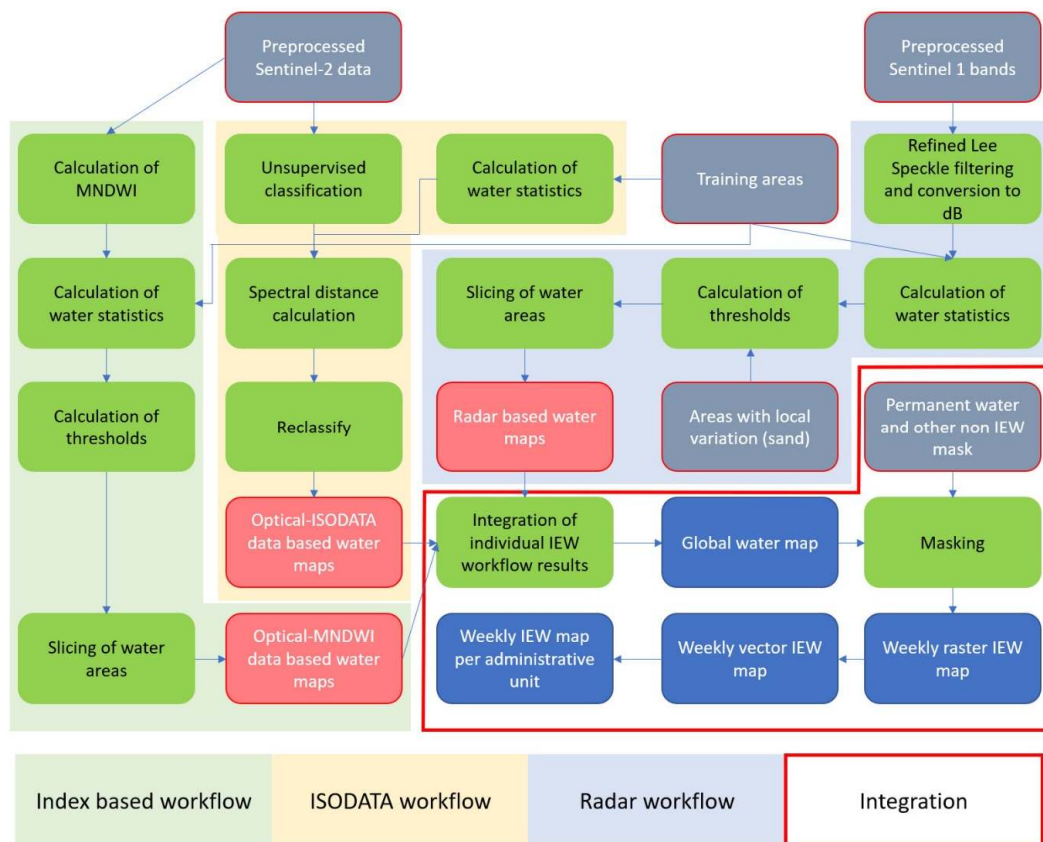

Figure 6. Inland excess water detection algorithm based on preprocessed Sentinel-1 and Sentinel-2 data (Van Leeuwen et al. 2020a).

The large number of satellite images and the complexity of the algorithm required full automation of the data processing workflows. Originally, separate models in different software packages were used to determine the IEW patches, but it turned out that it was impossible to manually execute all the steps within a reasonable timeframe (Van Leeuwen et al. 2017), hence a set of interlinked Python scripts was developed that combine standard libraries like gdal and numpy with arcpy for GIS operations (Van Leeuwen et al. 2020a). Two sets of scripts run with a different interval, automatically started using Windows Scheduler. The first set runs daily and is downloading, preprocessing and processing the active and passive satellite data in parallel for the Index, ISODATA and radar workflows, when new images become available. The second set runs on a weekly basis and integrates the daily results into the weekly map.

3.1. Downloading the base satellite data

Sentinel-1 and -2 data can be downloaded free of charge from ESA's Copernicus Open Access Hub. With the help of a python script, the GNU Wget program (www.gnu.org/software/wget) is called to log in to the Open Access Hub using user credentials and search for relevant Sentinel images. A list with images is returned and processed to extract the image URLs. These URLs are then fed to GNU Wget and the files are downloaded sequentially. If, due to overload of the ESA server or other reasons the file is not downloaded correctly, the process is restarted automatically after a predefined time interval. The script is restarted every day of the week that is processed, because sometimes data only becomes available a few days later instead of immediately after acquisition.

3.2. Preprocessing

Sentinel-1 data is preprocessed using the ESA SNAP graph processing tool (gpt) (http://step.esa.int/main/toolboxes/snap). An automated workflow was developed using a Python script to run a Sentinel-1 preprocessing graph within the ESA SNAP gpt (Figure 7) (Van Leeuwen et al. 2017). Each Sentinel-1 image is individually preprocessed to remove border and thermal noise and to optionally refresh geometry metadata based on the orbit information. The data is calibrated to sigma0 and filtered using a Refined Lee speckle filter to reduce the noise inherent to radar data. In the last step, the images are transformed using Rangle Doppler Terrain Correction to 10 x 10 meter images in UTM projection that can be combined with the other data sets. After the preprocessing phase, an additional step using a separate python script is performed to reduce the effect of the incidence angle on the backscatter values, by normalizing every pixel in the preprocessed image using the local incidence angle (Mladenova et al. 2013).
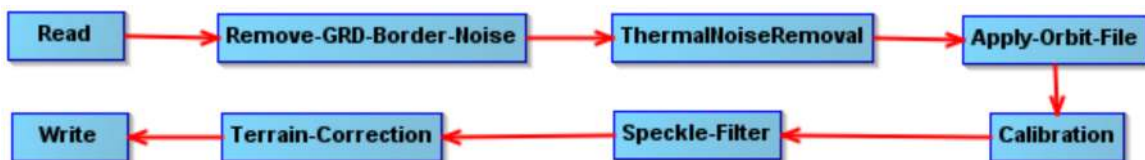

Figure 7. ESA SNAP gpt graph to preprocess Sentinel-1 GRD images to sigma0 data.

Depending on when the data was acquired, Sentinel-2 also needs to be processed since older data is only available in Level 1C top-of-atmosphere format. Level 1C data must be transformed into Level 2A bottom-of-atmosphere data using the Sen2Cor algorithm (https://step.esa.int/main/third-party-plugins-2/sen2cor). Once the data is in Level 2A format, selected spectral bands (Table 2) are resampled to 10 meter resolution, cloud masked and mosaiced using a custom python script that calls an ESA SNAP graph.

3.3. Processing
3.3.1. Radar based processing

The backscatter values of the preprocessed Sentinel-1 images are converted to decibel (db) units for easier handling in the processing workflow. The radar processing workflow is based on the basic assumption that the radar response of water is considerably lower than the response of other pixels. The challenge is to find the maximum backscatter value of water (Figure 8) (Bolanos et al. 2016, Liang & Liu 2020).
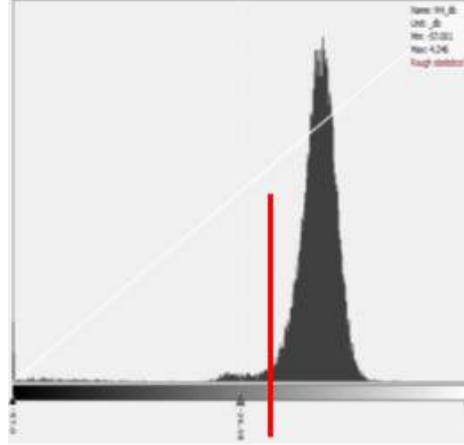

Figure 8. Histogram of a preprocessed Sentinel-1 VV band. The red line is showing the possible threshold between water and no water.

To determine this value, training data is collected for the VV and VH bands of a Sentinel-1 image. The training data consists of the statistics of the mask of known water bodies as described in 2.2.3. For each band, the minimum, mean and standard deviation of the water areas are determined. Based on these values, the upper and lower thresholds are calculated using an empirically determined method:

$$uthr_b = \bar{x} + k * \sigma, \tag{1}$$

$$lthr_b = x_{min} + (3 * (\bar{x} - x_{min})/5) \tag{2}$$

where
b is respectively band VV or VH,
$uthr_b$ is the upper threshold in db,
$lthr_b$ is the lower threshold in db,
$\bar{x}$ is the mean of the training samples in db,
x_{min} is the minimum of the training samples in db,
k is a user defined constant that can be adapted to specify the sensitivity of the algorithm to water. A higher number results in more pixels to be identified as water.

Sometimes, due to speckle or artifacts, pixels with very low backscatter values occur in the images. These pixels are excluded as water using the lower threshold. All pixels that are between the upper and lower thresholds in both bands are stored as water pixels:

$$water\ pixel = lthr_b < x < uthr_b \tag{3}$$

where x is the value of an individual pixel.

If the statistics of the training samples are beyond the normal range for example due to artifacts in the image, empirically determined standard values are used for the lower and upper thresholds. These are band specific ($lthr_{VV} = -40, uthr_{VV} = -17, \ lthr_{VH} = -50$ and $uthr_{VH} = -23$) because backscatter values for water are normally lower in the VH band. This is necessary to satisfy the requirement of full automation of the algorithm. Since each image is processed individually based on scene specific reference data, ascending and descending orbits are processed in the same way. It was observed that in areas with sandy soils, the backscatter values are lower resulting in overestimation of the amount of water pixels (Van Leeuwen et al. 2017). Therefore, an adaptation of the radar processing is applied to each sandy pixel in the image and the upper threshold is reduced by 25%. Pixels defined as water in both bands are considered water pixels and are stored in the final map. The result of the radar workflow is a binary map - clipped to the study area - showing all water in the area, whether it is an inland excess water inundation or a permanent water body like a lake or a river.

3.3.2. Optical data based classification

Open water surfaces are extracted from preprocessed mosaiced Sentinel-2 optical data using unsupervised ISODATA clustering. The statistics of the ISODATA output classes are compared with the statistics of the water class in the reference mask (see 2.2.3). The ISODATA classes that have the smallest spectral angle difference with the reference water are considered water (Kruse et al. 1993). The method requires a sufficient number of reference pixels, which is sometimes difficult to acquire due to cloud cover in the optical data. Therefore, a checking and verification step is implemented in the algorithm. In case of insufficient quantity of reference data, the Sentinel-2 classification is not performed. The classified raster is clipped to the study area and reclassified to a binary map, differentiating water and non-water pixels.

3.3.3. Optical data based index calculation and thresholding

The second workflow to extract water from the preprocessed and mosaiced Sentinel-2 data is based on the Modified Normalized Difference Water Index (MNDWI)(Xu 2005; Du et al. 2016). It is calculated from the green and Shortwave-Infrared (SWIR) bands, and it is one of the most popular methods to extract water pixels from multispectral satellite imagery. The index produces positive values for the water and negative values for built-up, soil and vegetation land cover:

$$MNDWI = \frac{\rho_{green} - \rho_{SWIR}}{\rho_{green} + \rho_{SWIR}} \qquad (4)$$

where
ρ_{green} and ρ_{SWIR} are the BoA reflectance of the green and SWIR bands resampled to a common 10 meter spatial resolution.

Water bodies are mapped by a slicing algorithm using a suitable threshold value. In general, the MNDWI value of a pixel larger than zero is considered as water. In practice, even though atmospherically corrected, multispectral images acquired at different regions and different times always have slightly different characteristics, thus the threshold can be empirically adjusted for the region and acquisition date using a multiplication factor:

$$MNDWI_{threshold} = MNDWI_{mean} - k * MNDWI_{std} \qquad (5)$$

where
$MNDWI_{mean}$ is the mean index value of the reference pixels,
$MNDWI_{std}$ is the standard deviation of the reference pixels,
k is a multiplication factor, its default value is 1.

If, due to cloud cover the number of pixels with reference data is very low, or the statistics are beyond the normal range, a standard value is used for Sentinel-2 MNDWI segmentation threshold. The result of the MNDWI index based workflow is a binary map – clipped to the study area - differentiating water from non-water pixels.

3.3.4. Integration

The binary maps produced by the three processing workflows cover different spatial areas and are from different dates during the week that is being processed. Data from different dates are aggregated into one weekly inland excess water map, because data from single date do not provide a reliable result (Van Leeuwen et al. 2017). To integrate the data and to determine the reliability of the final weekly inland excess water map, all individual partial result maps are extended to the total study area. Pixels where no information is available on whether there is water or not are designated -100. Pixels can get the -100 value, if they are cloud, shadow, outside the original image or for any other reason undetermined. The result is a large set of maps with three values: 0 (no water), 1 (water), and -100 (undetermined) covering the total study area (Figure 9).
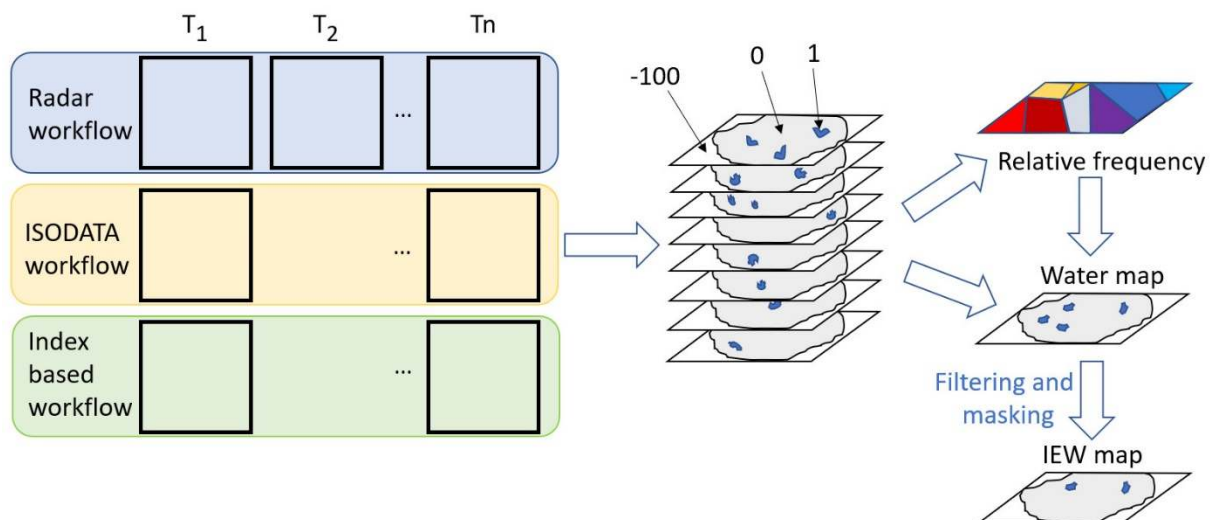

Figure 9. Integration process of the three parallel workflows

In the next step, a map is created storing the amount of times that it was determined if in a pixel there was water or no water. In another map, for each pixel, it is determined how many times water was found. By dividing the second map by the first map, a frequency map is created specifying the relative number of times water was found in a pixel compared to the number of times data was available. If the relative frequency of water is above the manually specified threshold (e.g. 0.4 or 40%), the pixel is determined to be water. This map is then filtered to delete single water pixels surrounded by no water pixels and to fill up individual no water pixels surrounded by water pixels. In this way, more continuous inundations are generated. In the final step, all known permanent water bodies are masked out based on the mask file (see 2.2.3) and a binary weekly inland excess water raster map is created. The raster map is vectorized and the inland excess water coverage in hectare is calculated for different administrative units.

3.3.5. Validation

Validation data for the 2016 inland excess water period were derived from a pan-sharpened multispectral SPOT-7 image. Water surfaces were extracted using automated clustering, combined with manual selection of water classes. From the classified raster, gaps and separated water pixels smaller or equal to the base resolution of the IEW monitoring workflow (10 x 10 m) were removed using the Sieve method. Permanent water bodies, linear infrastructures, built-up areas, and shadows were also removed. The 2018 validation was based on a 20 km^2 orthophoto mosaic. Inland excess water patches were visually identified and manually digitized. The resulting polygons were then rasterized to the resolution of the IEW monitoring workflow. The rasterized validation datasets and the weekly inland excess water maps were compared using cross-tabulation (Van Leeuwen et al. 2020a).

4. Results and discussion

Weekly inland excess water maps were created for the study area for two inland excess water periods in 2016 and 2018 (Figure 6). Parameters were fine-tuned to adjust the sensitivity of the algorithm to water but to remain within realistic boundaries. Visual inspection of the results, overlaying the IEW maps on different color composite of the Sentinel-2 input images shows that the algorithm properly delineates IEW inundations. The largest inundations are detected in regions with clayey soils with unfavorable water management characteristics and on the former floodplains, clearly showing the fluvial geomorphology like (former) oxbows and river meanders. The border of the Maros alluvial fan is clearly shown on the 2018 result, in fact even on its higher areas IEW is detected.
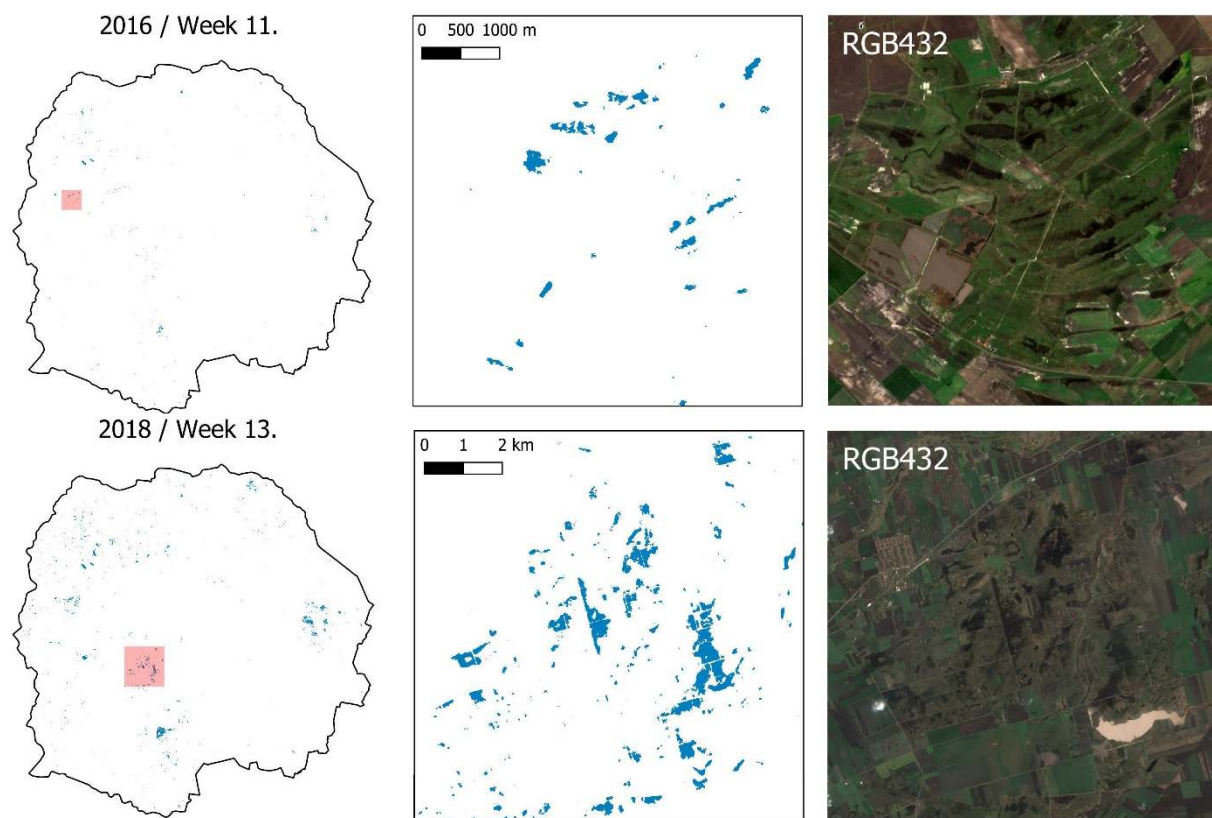

Figure 6. Detected inland excess water on the total study area (left) and on subareas (middle) in 11th week of 2016 (top) and in 13th week of 2018 (bottom) and natural color composites of the input optical data (right).

During the moderate IEW period of 2016, the algorithm detected a little over 600 ha of IEW mainly in the northwest and east parts of the total study area. More than half of the detected IEW polygons is small; not larger than 3 pixels (=< 300 m2). In 2016, 72% of the IEW patches detected by the algorithm consist of larger, minimum 1 ha big inundations, the largest patch is even larger than 25 ha. The results show that over half of the IEW inundations occur in agricultural areas, to a large extent on arable land, which has a substantial effect on the agricultural production. A further one third of the IEW patches is located on natural grassland.

In 2018, five times as much inland excess water was detected (3082 ha) as in 2016 and also the spatial distribution of the patches was more spread out than in the earlier research period. In fact, the floods have increased everywhere except on the higher regions of the central and south-eastern parts of the study area. The complexity of the issue of inland excess water formation and the importance of high-resolution monitoring was also demonstrated by the fact that in 2016, there were small IEW patches that were not inundated in 2018 (e.g. the arable land northwest of Orosháza).

In 2018, the chance of water detection within the period under investigation was larger than in 2016, since the number of available input images in 2018 was twice as high as in 2016, because in 2016 less satellites were in orbit than two years later. This issue only occurs in the earlier years of Sentinel acquisition when data from Sentinel-1B and Sentinel-2B was not yet available. In both years, the large and often deeper inundations that are part of non-permanent wetlands (in the south center and east) were detected almost perfectly.

Figure 7 shows a series of submaps of the detection result of 2018 from the northwest part of the study area. At the top, the figure shows that the three detection workflows detect similar patterns of water, but that there are some differences. The MNDWI based water map shows the most water, while the ISODATA based map is the least sensitive to water in this area.
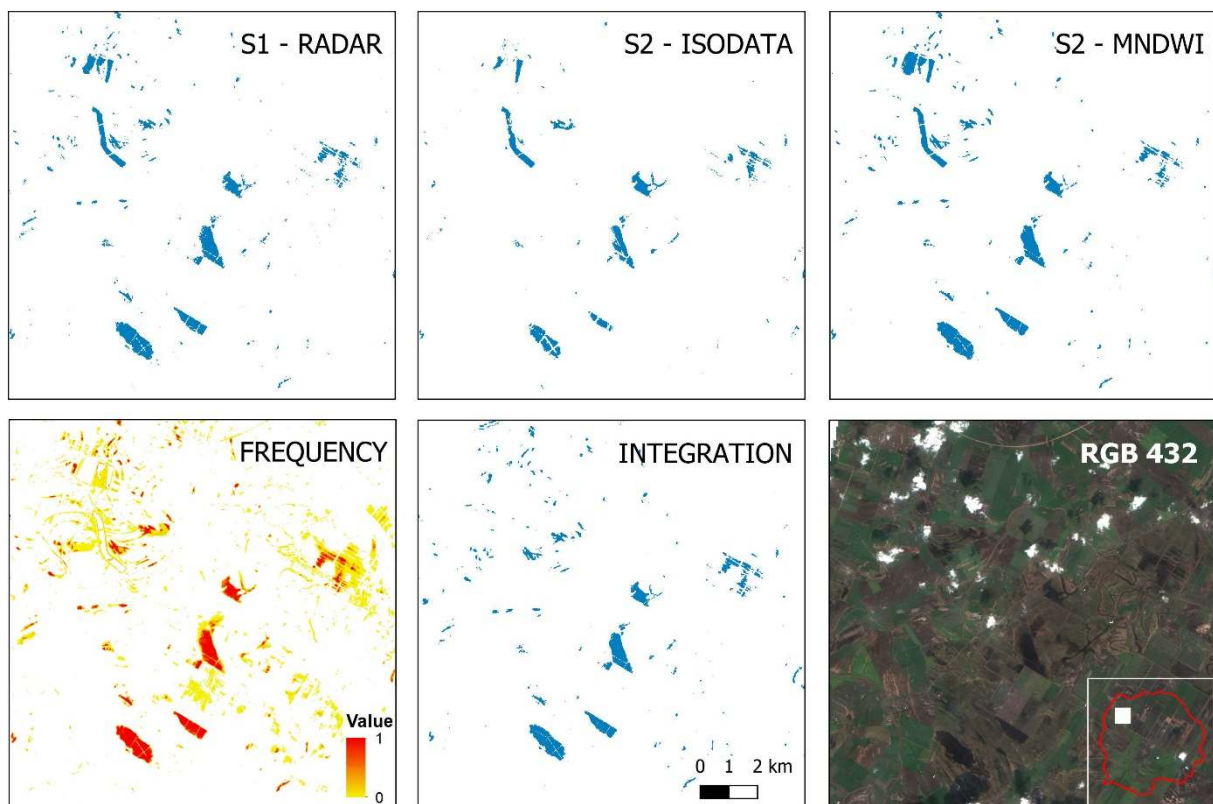

Figure 7. Sub-results of the different workflows (top row), frequency of water detection (bottom left), the integrated final inland excess water map (middle below) and the Sentinel-2 natural color composite with clouds and cloud shadows of a selected area in 13th week of 2018.

The frequency map shows for each pixel the ratio between the number of times water was detected in a pixel and the total amount of times the pixel was evaluated in the water detection process. This map can be used as a detection confidence map. It can be clearly seen that the deep waterbodies are detected most of the time, while more shallow water at the border of the deeper IEW patches is less often detected. These areas form the fuzzy boundary between water, saturated soil and dry land. The integration map stores only water pixels that are detected more often than the empirically defined relative frequency threshold, in other words, the integration map stored the pixels with the highest confidence of IEW.

Often cloud and cloud shadows have a disturbing influence on the IEW detection as can be seen on the northern half of the natural color composite. The algorithm takes this into account by masking the clouds and shadows in the optical data and ignoring these pixels in the relative frequency calculation. The cloud/shadow masking prevents the algorithm to derive IEW from affected pixels in the optical data, but since radar images are not influenced by atmospheric disturbance, these areas are evaluated for water by the active satellite data based workflow.

The results of the IEW water detection algorithm in 2016 were validated with the SPOT 7 image. The quantification of the validation is based on a pixel by pixel comparison between the SPOT image and the algorithm result and shows that the overall accuracy is high, but the Cohen's Kappa is low, due to very high omission error (Table 4). This is due to the fact that if one IEW patch is missed in the classification, a large number of pixels is misclassified and added to the omission error. Also, the classification is unbalanced due to the high amount of "no water", compared to "water" pixels.

	Reference				Producer's Acc.	Omission error	User's Acc.	Commission error
# pixels	no water	water	Total					
no water	4454908	7807	4462715		99.92	0.08	99.83	0.17
water	3494	4513	8007		36.63	63.37	56.36	43.64
Total	4458402	12320	4470722		Overall Acc.	99.74	Kappa	0.44

Table 4. Accuracy assessment on the validation site in 2016

The IEW inundations delineated for the 2018 period were validated using the high resolution orthophoto. From the orthophoto mosaic, 849 inland excess water patches - covering 147.5 ha - were digitized, however the algorithm only delineated 52 polygons (8.9 ha). As can be seen in Figure 8, large shallow inundations that were identifiable on the aerial photographs can hardly be seen on the Sentinel-2 image and were also omitted by the algorithm. Like in 2016, the deep/dark water patches are delineated almost perfectly.
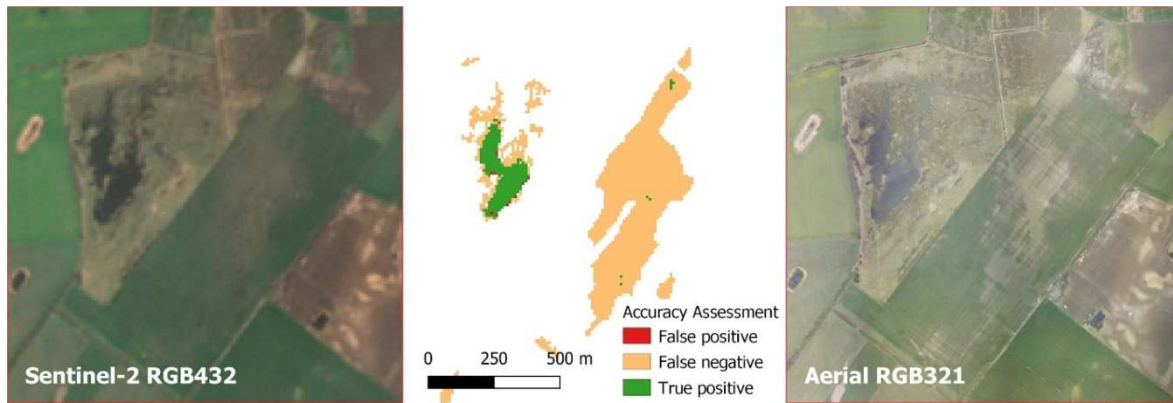
Figure 8. Results of the cross-validation on a selected area in 2018, with the Sentinel-2 natural color composite (used as input for the optical workflow) on the left, the weekly IEW map in the middle and the color aerial photograph (used for the validation) on the right.

The calculated accuracy and error values for the water class are shown in Table 5. They prove that the applied method indicates the occurrences of inundations to the user properly in almost every case (user accuracy is over 90%) however, the ratio of false negative cases is very high (omission error is over 90%).

	Reference							
# pixels	no water	water	Total		Producer's Acc.	Omission error	User's Acc.	Commission error
no water	185712	13919	199631		99.97	0.03	93.03	6.97
water	59	830	889		5.63	94.37	93.36	6.64
Total	185771	14749	200520		Overall Acc.	93.03	Kappa	0.10

(Detected — row label for the "no water / water / Total" rows)

Table 5. Accuracy assessment on the validation site in 2018

The difference between IEW identified by the algorithm and the reference data sets can also be caused by the difference in acquisition dates. The algorithm is developed to create weekly IEW maps, because earlier research showed that combining multiple daily results gives more accurate IEW maps (Van Leeuwen et al. 2017). The reference SPOT satellite data and aerial photographs are from a single moment in time, and because IEW is a fast-changing phenomenon, differences in acquisition date of several days can lead to changes in the IEW patches. This is particularly characteristic for the boundaries of the patches where the water infiltrated or evaporated in case of reduced IEW, or when the size of a patch increased due to extra water. This makes the validation of the weekly maps with single date reference data more difficult.

To better understand the difference between the IEW patches detected by the algorithm and the polygons delineated on the SPOT satellite image and aerial photographs, the number of inundations and their area were compared. It turns out that most of the reference polygons (over 70%) is in the smallest size range, however their cumulative area is not larger than 10% of the total inundation. Because of the difference between the image resolutions, the algorithm is not able to detect these small patches. In the larger size ranges, the statistics of the reference and the detected IEW patches are more similar.

The underestimation of the amount IEW patches/pixels by the algorithm can be reduced by changing the parameters for the threshold of the water detection by the radar data, the amount of ISODATA classes that show water and the threshold of the MNDWI slicing. Also, the threshold for the relative frequency required to assign a pixel as water can be set in the algorithm. It was decided to keep the parameters such that realist values remained for the thresholds and ISODATA water classes, and therefore excepting the underestimation. Extreme fine-tuning of the parameters may be possible for small areas but is not feasible since the algorithm is designed to work for large areas. Also, the algorithm is fully automated and runs without any user intervention. Fine-tuning of the parameters per area and time would prevent automation.

5. Conclusions

This habilitation thesis is the result of the accumulated work of my research performed on continuous monitoring of inland excess water since my PhD work in 2012. In this habilitation, I have presented an algorithm that can detect inland excess water on very large areas based on a combination of active and passive satellite imagery. The base data is freely available and can be downloaded with a high temporal resolution. The workflow is fully automated, so no human intervention is needed to generate the weekly IEW maps. Two IEW periods and an area sensitive to the phenomenon were selected to demonstrate and validate the methodology, but the algorithm can be applied to any area affected by this type of inundations. Using quantitative validation, I have shown that the weekly IEW detection algorithm based on medium optical and radar satellite data is capable of detecting the inundations, but compared to the validation data generated using high-resolution satellite data or aerial photographs, it underestimates the amount of IEW in the study area. This is primarily because the algorithm is not able to fully detect the smaller patches. Furthermore, intermediate IEW classes like soil saturated with water and IEW patches covered with vegetation are often not detected.

The extreme weather patterns that are expected in the Carpathian Basin in the near future due to climate change will increase the chance that IEW will develop more often and that its extent will be larger. Therefore, it is important to develop robust algorithms to map and monitor the phenomenon. The presented algorithm supports efficient water management activities to mitigate the negative effects of IEW and to increase the sustainable use of the surplus water in periods of deficit.

Currently, two versions of the presented algorithm are implemented in an operative environment. An earlier, simplified version has been implemented in the Földmegfigyelési Információs Rendszer (FIR) environment that runs at Lechner center. The second version is implemented at the Drought and Excess Water Research and Monitoring Centre at the Department of Physical Geography and Geoinformatics of the University of Szeged, where it produces weekly IEW maps on a regular basis (https://aszaly.geo.u-szeged.hu/wateratrisk/map/?locale=hu).

6. Acknowledgement

References

Baghdadi, N.; Bernier, M.; Gauthier, R.; Neeson, I., 2001. Evaluation of C-band SAR data for wetlands mapping. *International Journal of Remote Sensing 22*(1), 71–88, DOI: 10.1080/014311601750038857

Balázs B.; Bíró, T.; Dyke, G.; Singh S.K.; Szabó, Sz., 2018. Extracting water-related features using reflectance data and principal component analysis of Landsat images. *Hydrological Sciences Journal-Journal des Sciences Hidrologiques*, *63*(2), 269-284.

Binh Pham-Duc, B.; Prigent, C.; Aires, F., 2017. Surface water monitoring within Cambodia and the Vietnamese Mekong delta over a year with Sentinel-1 SAR observations. *Water 9*, 366; DOI:10.3390/w9060366

Bolanos, S.; Stiff, D.; Brisco, B.; Pietroniro, A., 2016. Operational surface water detection and monitoring using Radarsat-2, *Remote Sensing 8,* 285; DOI:10.3390/rs8040285

Bozán, Cs.; Körösparti, J.; Andrási, G.; Túri, N.; Pásztor, L., 2017. Inland excess water hazard on the flat lands in Hungary. C*olumella: Journal of Agriculture and Environmental Sciences 4*(1) (suppl), 45–48.

Bozán, Cs.; Körösparti, J.; Pásztor, L.; Kuti, L.; Kozák, P.; Pálfai, I., 2009. GIS-based mapping of excess water inundation hazard in Csongrád county (Hungary). In *Proceedings of the International Symposia on Risk Factors for Environment and Food Safety & Natural Resources and Sustainable Development*, 6-7 November: Faculty of Environmental Protection, Oradea, Romania, 678–684.

Bozán, Cs.; Pálfai, I.; Pásztor, L.; Kozák, P.; Körösparti, J., 2005. Mapping of Excess Water Hazard in Békés and Csongrád Counties of Hungary. In *Integrated Land and Water Resources Management: Towards Sustainable Rural Development*, Proceedings of ICID 21st European Regional Conference, Frankfurt (an Oder) and Slubice, Germany and Poland, p.4

Bozán, Cs.; Takács, K.; Körösparti, J.; Laborczi, A.; Túri, N.; Pásztor, L., 2018. Integrated spatial assessment of inland excess water hazard on the Great Hungarian Plain. *Land Degrad Dev. 29*, 4373–4386. DOI: 10.1002/ldr.3187

Chatziantoniou, A.; Psomiadis, E.; Petropoulos, G., 2017. Co-orbital Sentinel 1 and 2 for LULC mapping with emphasis on wetlands in a mediterranean setting based on machine learning. *Remote Sensing 9*(12), 1259 DOI: 10.3390/rs9121259

Clerici, N.; Augusto, C.; Calderón, V.; Posada, J.M., 2017. Fusion of Sentinel-1A and Sentinel-2A data for land cover mapping: a case study in the lower Magdalena region, Colombia. *Journal of Maps 13*(2), 718–726, DOI:10.1080/17445647.2017.1372316

Csekő, Á. 2003. Árvíz- és belvízfelmérés radar felvételekkel (Flood and inland excess water survey using radar imagery). *Geodézia és Kartográfia 2*, 16–22.

Csendes, B.; Mucsi, L., 2016. Inland excess water mapping using hyperspectral imagery. *Geographica Pannonica 20*(4), 191–196. DOI: 10.18421/GP20.04-01

Csornai, G.; Lelkes, M.; Nádor, G.; Wirnhardt, Cs., 2000. Operatív árvíz- és belvíz-monitoring távérzékeléssel (Remote sensing based operative flood and inland excess water monitoring). *Geodézia és Kartográfia 52*(5), 6–12.

Du, Y.; Zhang, Y.; Ling, F.; Wang, Q.; Li, W.; Li, X., 2016. Water bodies' mapping from Sentinel-2 imagery with Modified Normalized Difference Water Index at 10-m spatial resolution produced by sharpening the SWIR band. *Remote Sensing 8*, 354. DOI: 10.3390/rs8040354

ESA Sentinel Scientific Data Hub. 2020. Retrieved from. https://scihub.copernicus.eu/dhus/#/home

Gálya, B.; Riczu, P.; Blaskó, L.; Tamás, J., 2016. Belvíz érzékenység vizsgálata radar adatok alapján (Radar data based inland excess water sensitivity study), In *Theory meets practice in GIS*; Balázs, B. Ed; University of Debrecen, Hungary, 161–168.

Goffi, A.; Stroppiann, D.; Brivio, P.A.; Bordogna, G.; Boschetti, M., 2020. Towards an automated approach to map flooded areas from Sentinel-2 MSI data and soft integration of water spectral features. *Int. J. Appl. Earth Obs. Geoinformation 84*, 101951 DOI: 10.1016/j.jag.2019.101951.

Gulácsi, A.; Kovács, F., 2019. Radaralapú vizesélőhely-monitoring Sentinel-1 adatokkal. (Wetland monitoring based on Sentinel-1 imagery) *Hidrológiai Közlöny 99*(1), 38-47.

Hong, S; Jang, H; Kim N; Sohn, H-G., 2015. Water Area Extraction Using RADARSAT SAR Imagery Combined with Landsat Imagery and Terrain Information. *Sensors 6652-6667*, DOI:10.3390/s150306652.

Integrált vízháztartási tájékoztató (Integrated water management information) Aprilis 2016., General Directorate of Water Management, Budapest (in Hungarian) https://www.vizugy.hu/uploads/csatolmanyok/1271/vhte-1604-kivonat.pdf. [2020.22.10]

Integrált vízháztartási tájékoztató (Integrated water management information) Aprilis 2018., General Directorate of Water Management, Budapest (in Hungarian) https://www.vizugy.hu/uploads/csatolmanyok/1467/vhte-1804-kivonat.pdf. [2020.22.10]

Kozák P., 2006. A belvízjárás összefüggései az Alföld délkeleti részén, különös tekintettel a vízkárelhárítás európai igényeire (The evaluation of the excess surface waters on the Hungarian lowland's south-east part, in the expectation of the water management in Europe). Doktori Értekezés, SZTE Földtudományi Doktori Iskola, 86 p.

Kozma, Zs., 2019. A síkvidéki hidrológia és a belvíz vizsgálata folyamatalapú modellezéssel: kihívások és lehetőségek (Investigation of lowland hydrology and inland excess water with process-based modeling: challenges and opportunities). *Hidrológiai Közlöny 99*(2).

Kruse, F.; Lefkoff, A.B.; Boardman, J.; Heidebrecht, K.B.; Shapiro, A.T.; Barloon, P.J.; Goetz, A., 1993. The Spectral Image Processing System (SIPS)-Interactive Visualization and Analysis of Imaging Spectrometer Data. *Remote Sensing of Environment 44*, 145–163. DOI: 10.1016/0034-4257(93)90013-n

Ladányi, Zs.; van Leeuwen, B.; Blanka, V.; Tobak, Z.; Kovács, F.; Mezősi, G., 2019. Monitoring of drought and inland excess water in the serbian-Hungarian cross-border regi-on in the first half-year of 2019., In: Alapi, Tünde; Ilisz, István (szerk.) Proceedings of the 25th International Symposium on Analytical and Environmental Problems, Szeged, Magyarország: University of Szeged, pp. 325-329.

Liang, J.; Liu, D., 2020. A local thresholding approach to flood water delineation using Sentinel-1SAR imagery. *ISPRS Journal of Photogrammetry and Remote Sensing 159*, 53–62.

Licskó, B.; Vekerdy, Z.; Szilágyi, A.; Busics, I., 1987. *Távérzékelési módszertani útmutató a meliorációs tanulmánytervek készítéséhez (Handbook for remote sensing methodology for the preparation of land improvement plans)*, Földmérési és Távérzékelési Intézet, Budapest.

Liu, C., 2016. Analysis of Sentinel-1 SAR Data for Mapping Standing Water in the Twente Region. Master Thesis, ITC. Enschede. The Netherlands.

Malenovský, Z.; Rott, H.; Cihlar, J.; Schaepman, M.E.; García-Santos, G.; Fernandes, R.; Berger, M., 2012. Sentinels for science: Potential of Sentinel-1, -2, and -3 missions for scientific observations of ocean, cryosphere, and land. *Remote Sensing of Environment 120*, 91–101. DOI: 10.1016/j.rse.2011.09.026

Manjusree, P.; Prasanna Kumar, L.; Bhatt, C.M.; Rao, G.S.; Bhanumurthy, V., 2012. Optimization of Threshold Ranges for Rapid Flood Inundation Mapping by Evaluating Backscatter Profiles of High Incidence Angle SAR Images, *Int. J. Disaster Risk Sci. 3* (2): 113–122, DOI:10.1007/s13753-012-0011-5

Mezősi, G., 2017. *Physical geography of Hungary*. Springer International Publishing, p.334.

Mezősi G.; Burghard C.M.; Wolfgang, L.; Christoph, A.; Peter, Cs.; Teodora, B., 2013. Assessment of regional climate change impacts on Hungarian landscapes. *Reg Environ Change 13*, 797–811. DOI: 10.1007/s10113-012-0326-1

Mladenova, I. E.; Jackson, T. J.; Bindlish R.; Hensley, S., 2013. Incidence Angle Normalization of Radar Backscatter Data. *IEEE Transactions on Geoscience and Remote Sensing 51* (3), 1791-1804. DOI: 10.1109/TGRS.2012.2205264.

Mucsi, L.; Henits, L., 2010. Creating excess water inundation maps by sub-pixel classification of medium resolution satellite images. *Journal of Environmental Geography 3*(1–4), 31–40.

Nađ, I.; Marković, V.; Pavlović, M.; Stankov, U.; Vuksanović, G., 2018. Assessing inland excess water risk in Kanjiza (Serbia), *Geografie-Sbornik Ceske Geograficke Spolecnosti 123*(2), 141-158.

Pálfai I., 2000. Az Alföld belvízi veszélyeztetettsége és aszályossága. In: (Eds), A víz szerepe és jelentősége az Alföldön. A Nagyalföld Alapítvány Kötetei 6., Békéscsaba, pp. 85 - 95.

Pálfai, I., 2001. A belvíz definíciói (Definitions of inland excess waters). *Vízügyi Közlemények 83*(3), 376–392.

Pálfai I., 2003. Magyarország belvíz-veszélyeztetettségi térképe (Hungarian inland excess water map). *Vízügyi közlemények 85*(3), 510–524.

Pásztor, L.; Körösparti, J.; Bozán, Cs.; Laborczi, A.; Takács, 2015. K. Spatial risk assessment of hydrological extremities: Inland excess water hazard, Szabolcs-Szatmár-Bereg County, Hungary. *Journal of Maps 11*(4), 636–644. DOI: 10.1080/17445647.2014.954647.

Rakonczai, J.; Farsang, A.; Mezősi, G.; Gál, 2011. N. A belvízképződés elméleti háttere (Conceptual background to the formation of inland excess water). *Földrajzi Közlemények 35*(4), 339–350.

Rakonczai, J.; Mucsi, L.; Szatmári, J.; Kovács, F.; Csató, Sz., 2001. A belvizes területek elhatárolásának módszertani lehetőségei (Methods for delineation of inland excess water areas). *A földrajz eredményei az új évezred küszöbén. Az I. Magyar Földrajzi Konferencia CD*, p.14.

Slagter, B.; Nandin-Erdene, T.; Andreas, V.; Johannes, R., 2020. Mapping wetland characteristics using temporally dense Sentinel-1 and Sentinel-2 data: A case study in the St. Lucia wetlands, South Africa. *Int. J. Appl. Earth Obs. Geoinformation 86*, 102009.

Steinhausen, M.J.; Wagner, P.D.; Narasimhand, B.; Waske, B., 2018. Combining Sentinel-1 and Sentinel-2 data for improved land use and land cover mapping of monsoon regions. *Int. J. Appl. Earth Obs. Geoinformation 73*, 595–604.

Szatmári, J.; Kovács, F.; van Leeuwen, B.; Tobak, Z., 2020. Belvízelöntések vizsgálata távérzékeléssel a 2000-es években a Szegedi Tudományegyetemen (Investigation of inland excess water by remote sensing in the 2000s at the University of Szeged), In: Farsang, Andrea; Ladányi, Zsuzsanna; Mucsi, László (szerk.) Klímaváltozás okozta kihívások: Globálistól lokálisig, Szeged, Magyarország: SZTE TTIK Földrajzi és Földtudományi Intézet, pp. 71-81.

Szatmári, J.; van Leeuwen, B., 2013. *Inland Excess Water – Belvíz – Suvišne Unutrašnje Vode*, Szeged; Újvidék: Szegedi Tudományegyetem; Újvidéki Egyetem, p.154.

Tobak, Z.; Szatmári, J.; Van Leeuwen, B.; Minučer, M.; Mucsi, L., 2014a. Az időszakos felszíni vízborítások (belvíz) térbeli és időbeli megjelenésének monitoringja =. Prostorni i vremenski monitoring pojave = Monitoring spatial and temporal apperance of temporary surface water covers, In: Blanka, Viktória; Ladányi, Zsuzsanna (szerk.) Aszály és vízgazdálkodás a Dél-Alföldön és a Vajdaságban = Suša i upravljanje vodama u južnoj mađarskoj ravnici i Vojvodina = Drought and water management in South Hungary and Vojvodina, Szeged, Magyarország: SZTE TTIK Természeti Földrajzi és Geoinformatikai Tanszék, pp. 273-279.

Tobak, Z.; Van Leeuwen B.; Henits, L.; Szatmári, J., 2014b. Satellite-based inland excess water flood detection, In: Marko, Cvetkovic; Kristina, Novak Zelenika; János, Geiger (szerk.) 6th Croatian - Hungarian and 17th Hungarian geomathematical congress: Geomathematics - from theory to practice, Zagreb, Horvátország: Croatian Geological Society, pp. 139-144.

Tobak, Z.; van Leeuwen, B.; Kovács, F.; Szatmári, J., 2019. Belvíz elöntések nagy pontosságú térképezése és monitorozása = Monitoring i kartiranje plavljenja unutrašnjim vodama sa velikom tačnošću = High precision mapping and monitoring of inland excess water inundations, In: Ladányi, Zsuzsanna; Blanka, Viktória (szerk.) Aszály és belvíz monitoring és menedzsment, valamint a kapcsolódó kockázatok a Dél-Alföldön és a Vajdaságban, Szeged, Magyarország: Szegedi Tudományegyetem Természeti Földrajzi és Geoinformatikai Tanszék, pp. 13-22.

Tavares, P.A.; Beltrão, N.E.S.; Guimarães U.S.; Teodoro, A.C., 2019. Integration of Sentinel-1 and Sentinel-2 for Classification and LULC Mapping in the Urban Area of Belém, Eastern Brazilian Amazon. *Sensors 19*, 1140, DOI:10.3390/s19051140.

Van Leeuwen, B., 2012. Artificial neural networks and geographic information systems for inland excess water classification, PhD Dissertation, Earth Sciences Doctoral School, University of Szeged, 106 p.

Van Leeuwen B.; Henits, L.; Minucsér, M.; Szatmári, J.; Tobak, Z.; Dragoslav, P.; Stevan, S., Dragan, D., 2013. Belvíz-elöntések lehatárolása RapidEye műhold-felvételek alapján, *Hidrológiai Közlöny 93* (3), pp. 17-24.

Van Leeuwen, B.; Tobak, Z., 2014. Operational Identification of Inland Excess Water Floods Using Satellite Imagery, In: Robert, Vogler; Adrijana, Car; Josef, Strobl; Gerald, Griesebner (szerk.)

GI_Forum 2014 – Geospatial Innovation for Society, Salzburg, Ausztria: Herbert Wichmann Verlag im Verlag VDE GmbH, pp. 12-15.

Van Leeuwen, B.; Henits, L.; Minucsér, M.; Tobak, Z.; Szatmári, J., 2013. RapidEye satellite imagery for inland excess water identification, In: Lóki, József (szerk.) Az elmélet és a gyakorlat találkozása a térinformatikában IV.: Térinformatika Konferencia és Szakkiállítás, Debrecen, Magyarország : Debreceni Egyetemi Kiadó, pp. 465-472.

Van Leeuwen, B.; Mezősi, G.; Tobak, Z.; Szatmári, J.; Barta, K., 2012. Identification of inland excess water floodings using an artificial neural network. *Carpathian Journal of Earth and Environmental Sciences 7* (4), 173–180.

Van Leeuwen, B.; Právetz, T.; Liptay, Z.A.; Tobak, Z., 2016. Physically based Hydrological Modelling of Inland Excess Water. *Carpathian Journal of Earth and Environmental Sciences 11* (2), 497–510.

Van Leeuwen B.; Tobak Z.; Kovács F., 2020a. Sentinel 1 and 2 based near real time inland excess water mapping for optimized water management, *Sustainability* 12 (7), Paper: 2854, 21 p.

Van Leeuwen, B.; Tobak, Z.; Kovács, F., 2020b. Machine Learning Techniques for Land Use/Land Cover Classification of Medium Resolution Optical Satellite Imagery Focusing on Temporary Inundated Areas, *Journal of Environmental Geography* 13 (1-2), pp. 43-52.

Van Leeuwen, B.; Tobak, Z.; Kovács, F.; Sipos, Gy., 2017. Towards a continuous inland excess water flood monitoring system based on remote sensing data. *Journal of Environmental Geography 10*(3-4), pp. 9-15.

Xu, H., 2005. A study on information extraction of water body with the modified normalized difference water index (MNDWI), *International Journal of Remote Sensing 5*, 589-595. DOI: 10.1080/01431160600589179